Pergamon

Int. Comm. Heat Mass Transfer, Vol. 26, No. 7, pp. 997–1007, 1999

0735-1933/99/$–see front matter

PII S0735-1933(99)00089-5

SCALING ANISOTROPIC SCATTERING IN RADIATIVE TRANSFER IN THREE-DIMENSIONAL NONHOMOGENEOUS MEDIA

Zhixiong Guo and Shigenao Maruyama
Institute of Fluid Science, Tohoku University, Sendai 980-8577, Japan

(Communicated by K. Suzuki and S. Nishio)

ABSTRACT

Radiative heat transfer in three-dimensional nonhomogeneous participating medium was investigated by using REM^2 method. The anisotropic scattering phase function was dealt with the scaling technique based on delta function approximation. The three-dimensional scaled isotropic results were compared with the published anisotropic scattering computations. A good agreement between the scaled isotropic approaches and the anisotropic solutions was found. The effects of scattering albedo, forward fraction of phase function, and wall emissivity were discussed. It was found that, with the increase of the scattering albedo, the radiative heat flux increases for forward scattering media, but decreases for backward scattering media. The radiative heat flux is increased with the increases of forward fraction of phase function and wall emissivity. The emissive power at the center of a cubical nonhomogeneous medium in radiative equilibrium with gray diffuse walls equals to the averaged blackbody emissive power of the six walls.

Introduction

Radiative heat transfer in three-dimensional nonhomogeneous participating media is a problem of practical significance with wide applications to such systems as industrial furnaces and combustion chambers. Anisotropic scattering from particulate matter is usually a basic feature in such kinds of systems. As Kim and Lee [1] point out, however, full anisotropic modeling of multidimensional radiative transfer in an anisotropic scattering medium requires a large amount of computer time and storage. Scaling is a widely used scheme for obtaining rapid yet accurate radiative transfer results for anisotropic scattering media. Lee and Buckius [2] have shown that scaling laws allow some anisotropic scattering problems to be reduced to, and solved as, isotropic scattering problems.

There have been many attempts at scaling the complex anisotropic scattering problem. Wiscombe [3] has proposed the δ-M method for scaling the phase function into either isotropic or simple anisotropic

scattering. The delta-Eddington approximation is developed by Joseph *et al.* [4]. An excellent review by McKellar and Box [5] has summarized the previous works on scaling techniques. Recently, radiative transfer in a planar medium with anisotropic scattering is scaled to an isotropic scattering problem by the P_1 approximation [2], in which the accuracy of the scaling laws for one-dimensional problem has been demonstrated. More recently, scaled isotropic scattering solutions are compared with the full anisotropic scattering solutions of the radiative heat transfer in a two-dimensional homogeneous medium by Kim and Lee [1]. The isotropic scaling approximation was found to predict accurately the radiative heat flux. Maruyama [6] has applied the zeroth-order delta function approximation using REM^2 method for the case of plane parallel system with very good accordance with the exact solution even for strong forward or backward scattering particles. A literature survey reveals, however, that the isotropic scaling approximation has not been compared with the anisotropic scattering solutions in three-dimensional media. Moreover, nonhomogeneous medium was not considered in the previous multi-dimensional scaled isotropic calculations. It is necessary to verify the scaled isotropic scattering radiative heat transfer in three-dimensional nonhomogeneous media.

The calculation of radiative heat transfer in complex three-dimensional configurations is still a difficult task. When the discrete ordinate method is applied to a complex 3D engineering model, for example, the ray effect [7] is unavoidable. Among numerous solution methods, the radiation element method by ray emission method, REM^2, is flexible to deal with arbitrary three-dimensional geometry. The REM^2 method developed by Maruyama [8] and Maruyama and Aihara [9] may analyze radiative transfer in participating media and specular and/or diffuse surfaces in arbitrary configurations as easily as the finite element analysis. This method has been applied to complex configurations such as a large device for the research of a fusion reactor [10], and Czochralski and floating zone furnaces for crystal growth [11,12]. The REM^2 method has been developed to incorporate nongray and anisotropic scattering properties by Maruyama *et al.* [13] and Guo and Maruyama [14]. However, an instinctive limitation in REM^2 method is that it requires an isotropic scattering phase function, while most scattering particles are anisotropic scattering media. This limitation may be overcome by using isotropic scaling technique, which also motivates the present study.

In this treatise, the isotropic scaling radiative heat transfer in a three-dimensional nonhomogeneous medium with anisotropic scattering and absorbing and emitting is investigated using the REM^2 method. The zeroth-order delta function approximation is used to scale the anisotropic scattering into isotropic scattering. The accuracy of the scaled isotropic calculations is verified by comparison with the available published solutions of anisotropic scattering. The effects of scattering albedo, forward fraction of phase function, and wall emissivity on radiative heat transfer are discussed. A relationship, which is valid for homogeneous medium covered with black walls, is examined for nonhomogeneous medium with gray diffuse walls.

Mathematical Model

The phase function may be expressed in terms of Legendre polynomials as

$$\Phi(\mu)=\sum_{n=0}^{\infty} a_n P_n(\cos\mu) \tag{1}$$

For many calculations the above expression is so complicated that so-called *Dirac-delta* approximation is adopted as follows:

$$\Phi(\mu)\approx 2f\delta(1-\cos\mu)+(1-f)\Phi^*(\mu) \tag{2}$$

The approximate phase function is expressed as a truncated Legendre series,

$$\Phi^*(\mu)=1+\sum_{n=1}^{M} a_n^* P_n(\cos\mu) \tag{3}$$

If Φ^* is to be isotropic, i.e., $M = 0$, the forward fraction of the phase function is then $f = a_1/3$, and the phase function is approximated by

$$\Phi(\mu)\approx 2f\delta(1-\cos\mu)+(1-f) \tag{4}$$

For any given anisotropic scattering phase function, we can scale it into isotropic scattering as follows:

$$\beta^*=\beta(1-f\Omega),\quad \Omega^*=\frac{\Omega(1-f)}{1-f\Omega}. \tag{5}$$

After introducing the scaled isotropic phase function, the equation of radiative transfer in absorbing, emitting and scattering gray medium can be written as

$$\frac{dI(\vec{r},\omega)}{dS}=-\beta^*\left[I(\vec{r},\omega)+(1-\Omega^*)I_b(T)+\frac{\Omega^*}{4\pi}\int_{4\pi} I(\vec{r},\omega')\,d\omega'\right]. \tag{6}$$

We assume that the scattering radiation is distributed uniformly over a radiative element, and introduce an averaged diffuse radiant intensity I^D [6]. The equation of transfer can be expressed by

$$\frac{dI(\vec{r},\omega)}{dS}=\beta^*\left[-I(\vec{r},\omega)+(1-\Omega^*)I_b(T)+\Omega^* I^D\right]. \tag{7}$$

If the scaled albedo Ω^* is redefined as Ω^D and the specular reflectivity of surface element Ω^S is defined, a generalized form of the radiant energy of element i, which may be either a volume or a surface element, can be expressed as

$$Q_{J,i}(\hat{s})=\left[(1-\Omega_i^D-\Omega_i^S)I_{b,i}(T_i)+\Omega^D I_i^D\right]\int_{A_i(\hat{s})}\left[1-\exp(-\int_0^S \beta_i^* dS)\right]d\omega\,dA \tag{8}$$

where $\int_0^S \beta_i^* dS >> 1$ stands for a surface element and $\Omega_i^S = 0$ for a volume element, respectively.

To simplify the integration in Eq. (8), an effective radiation area A_i^R is introduced:

$$A_i^R=\frac{1}{\pi}\int_{A_i(\hat{s})}\left[1-\exp(-\int_0^S \beta_i^* dS)\right]d\omega\,dA\approx\frac{1}{\pi}\int_{4\pi} A_i(\hat{s})\left[1-\exp(-\int_0^{\bar{S}} \beta_i^* dS)\right]d\omega \tag{9}$$

where an averaged thickness of the radiation element in the direction $\hat{s}$ is set to be $\bar{S} \equiv V / A(\hat{s})$. The rate of radiation energy emitted and scattered isotropically by the radiation element can be expressed in a generalized form as

$$Q_{J,i} \equiv A_i^R \left(\varepsilon_i E_{b,i} + \Omega_i^D G_i \right) \tag{10}$$

where $\varepsilon_i = 1 - \Omega_i^D - \Omega_i^S$, $E_{b,i} = \pi I_{b,i}$, $G_i = \pi I_i^D$, and $Q_{J,i}$ is the diffuse radiation transfer rate. The net rate of heat generation can be derived from the heat balance on the radiation element as

$$Q_{X,i} = A_i^R \varepsilon_i \left(E_{b,i} - G_i \right). \tag{11}$$

The emissive power of element is defined as $Q_{T,i} = A_i^R \varepsilon_i E_{b,i}$. If a system is consisted of N elements, then Eqs. (10) and (11) can be rewritten as

$$\left.\begin{aligned} Q_{J,i} &= Q_{T,i} + \sum_{j=1}^{N} F_{j,i}^D Q_{J,j} \\ Q_{X,i} &= Q_{T,i} - \sum_{j=1}^{N} F_{j,i}^A Q_{J,j} \end{aligned}\right\} \tag{12}$$

in which, the absorption view factor $F_{i,j}^A$ and diffuse scattering view factor $F_{i,j}^D$ are introduced as defined by Maruyama and Aihara (1997). Either the heat transfer rate of emissive power $Q_{T,i}$ or the net rate of heat generation $Q_{X,i}$ for each radiation element can be specified as a boundary condition. The unknown $Q_{X,i}$ and $Q_{T,i}$ can be attained by solving Eq. (12). Each radiation element is assumed to be homogeneous, but the medium as a whole may be nonhomogeneous. The view factors are calculated by using ray tracing method based on ray emission model as described by Maruyama and Aihara [7]. The discrete directions were distributed uniformly over the entire solid sphere.

Results and Discussion

Evaluation of Scaled Isotropic Results

The scaled isotropic results of radiative transfer in a cubic nonhomogeneous medium are evaluated by benchmark comparisons with the anisotropic scattering predictions by YIX and Monte Carlo methods [15]. The optical thickness (τ = extinction coefficient times the side length) distribution is given by

$$\tau = a\left(1 - \frac{|x|}{0.5}\right) \cdot \left(1 - \frac{|y|}{0.5}\right) \cdot \left(1 - \frac{|z|}{0.5}\right) + b \tag{13}$$

A linear anisotropic scattering phase function is assumed:

$$\Phi(\mu) = 1 + a_1 P_1(\cos\mu) \tag{14}$$

where P_1 is the first-order term of Legendre series.

TABLE 1

Conditions of Different Benchmark Cases

CASE	Ω	a_1	Constants in Eq. (13)	Boundary conditions
C1	0.9	1.	$a = 0.9, b = 0.1$	1 hot/5 cold walls
C2	0.9	-1.	$a = 0.9, b = 0.1$	1 hot/5 cold walls
C3	0.9	1.	$a = 5.0, b = 5.0$	1 hot/5 cold walls

TABLE 2

Comparison of the surface heat flux at $x = -0.5$ and $y = 0$ for cases C1 and C2, based on the present, YIX, and Monte Carlo methods.

CASE	C1			C2		
z	Present	YIX	M.C.	Present	YIX	M.C.
-4/9	0.98482	0.98586	0.98490	0.97130	0.96680	0.96560
-3/9	0.97806	0.98112	0.98010	0.95909	0.95218	0.95100
-2/9	0.97217	0.97706	0.97620	0.94838	0.93944	0.93870
-1/9	0.96776	0.97360	0.97310	0.94044	0.92947	0.92950
0	0.96572	0.97170	0.97170	0.93672	0.92465	0.92530

TABLE 3

Comparison of the emissive powers at $y = z = 0$ for cases C1 and C2, based on the present, YIX, and Monte Carlo methods.

CASE	C1			C2		
x	Pesent	YIX	M.C.	Present	YIX	M.C.
-4/9	0.46364	0.50679	0.46100	0.47412	0.52294	0.47660
-3/9	0.36786	0.36282	0.36640	0.37744	0.37710	0.37990
-2/9	0.28652	0.28177	0.28420	0.29368	0.29267	0.29450
-1/9	0.21962	0.22135	0.21830	0.22364	0.22730	0.22430
0	0.16637	0.17049	0.16650	0.16644	0.17050	0.16640
1/9	0.12672	0.11959	0.12580	0.12212	0.11505	0.12120
2/9	0.09785	0.09547	0.09642	0.09108	0.08914	0.08987
3/9	0.07552	0.06832	0.07516	0.06842	0.06159	0.06820
4/9	0.05814	0.06417	0.05986	0.05160	0.05795	0.05326

The coordinate origin lies at the center of the cube and the side length of the cube is unity. The constants in Eqs. (13) and (14), the scattering albedo and boundary conditions for bench mark comparisons are listed in Table 1. Cases C1 and C2 represent forward and backward scatterings in an intermediate optical thickness medium, respectively, while case C3 represents an optically thick medium. For all cases, the hot wall is set at $x = -0.5$, in which unity blackbody emissive power is given. All the walls are black. The medium is assumed to be in radiative equilibrium. The dimensionless variables in the following sections are defined by the side length (L) of the cube and the possible maximum heat flux

(σT_h^4) at the hot face.

In all cases, the cubic medium is divided into $9\times9\times9$ volume elements and each wall has 9×9 surface elements. In case C3, an additional solution is obtained for $19\times19\times19$ volume elements in order to improve the accuracy.

For cases C1 and C2, the predicted surface heat flux and emissive power are given in Tables 2 and 3 respectively. Comparisons are performed among the scaled isotropic calculations by REM^2 method and the published anisotropic results by YIX and Monte Carlo methods [15]. The general difference of the radiative heat flux between the present scaled approach and the Monte Carlo and YIX methods are 1%. The difference of the emissive power between the scaled results by REM^2 method and the anisotropic results by Monte Carlo method is less than 1%. The differences between the present approach and Monte Carlo method are smaller than the differences between the YIX and Monte Carlo methods in Table 3. As Hsu and Farmer [15] pointed out, this may be attributed to the ray effect occurring in YIX solutions. In the present approach, 2141 rays are employed in all computations to minimize the ray effect. While only 288 discrete directions were used in YIX method.

Table 4 summarizes the results for case C3 obtained based on the present method along with the available data by YIX and Monte Carlo methods. Two element grids are adopted in the present method. It is found that the present scaled results are in good agreement with the predictions of YIX and Monte Carlo methods. In the case of $9\times9\times9$ volume element grid, the averaged relative error between the present heat flux and those of Monte Carlo is 3%. When a finer element grid ($19\times19\times19$) is used, the averaged difference between the present approach and the Monte Carlo method is 1%. The difference of emissive power between those methods is larger than that of surface heat flux, but still in a range of 2%.

From the above comparisons, we may conclude that the scaled isotropic results are in good agreement with the anisotropic scattering calculations for three-dimensional nonhomogeneous absorbing, emitting and scattering media. The ray effect, which is often occurred in numerical methods with discrete directions, may be minimized in the REM^2 method since a large number of rays can be employed.

All the computations are performed with a VT-Alpha/533 personal computer. The CPU time in REM^2 method is consisted of two parts. One is the CPU time for the calculation of view factors, which is linearly proportional to the ray emission number in a personal computer. Another part is the CPU time used for the solution of Eq. (12), which is a main contribution to the total CPU time, especially in the case of a large number of radiation elements. In case C1, a total of 1215 radiation elements are employed and the ray emission number for each element is 2141. The calculation CPU time is 265 seconds, in which 44 seconds is consumed by the ray tracing process, and 221 seconds is used for the solution of Eq. (12) which involved two matrix inversions [8]. If the computational domain is axisymmetric, we may introduce the perfectly reflected elements along the axes, so that the number of radiation elements can be reduced. For example, we can introduce two perfectly reflected surfaces along the faces of $y = 0$ and $z =$

0 in the case of C1. The one-fourth computational domain can be divided into $9\times5\times5$ volume elements. The total CPU time is considerably reduced to 14 seconds.

TABLE 4

Comparison of the present, YIX, and Monte Carlo methods for case C3:

(a) surface heat flux at x = -0.5 and y = 0; (b) emissive power at $y = z = 0$.

z	Pesent (Scaled) $9\times9\times9$ vol. elements	Present (Scaled) $19\times19\times19$ vol. elements	YIX (LAS) $27\times27\times27$ grid	M.C. (LAS) $9\times9\times9$ grid
-4/9	0.73200	0.71832	0.72862	0.73260
-3/9	0.63548	0.61577	0.62774	0.62550
-2/9	0.58101	0.56258	0.57357	0.56670
-1/9	0.55319	0.53305	0.54266	0.53450
0	0.54255	0.52257	0.53151	0.52340

x	Pesent (Scaled) $9\times9\times9$ vol. elements	Present (Scaled) $19\times19\times19$ vol. elements	YIX (LAS) $27\times27\times27$ grid	M.C. (LAS) $9\times9\times9$ grid
-4/9	0.61976	0.63491	0.64099	0.64420
-3/9	0.46434	0.47553	0.47755	0.48220
-2/9	0.33998	0.34668	0.34883	0.35100
-1/9	0.24207	0.24506	0.24702	0.24700
0	0.16659	0.16653	0.16740	0.16640
1/9	0.11075	0.10880	0.10854	0.10760
2/9	0.07287	0.07037	0.06940	0.06878
3/9	0.04683	0.04437	0.04358	0.04310
4/9	0.02882	0.02566	0.02548	0.02484

Parameter Influence

Study of the influence of parameters such as the wall emissivity, scattering albedo, and forward fraction of phase function is sparse for three-dimensional nonhomogeneous medium. In order to investigate the influence of radiative parameters on the radiative heat transfer, we still consider the unit cube model specified above, but with a = 1.0 and b = 1.0 in Eq. (13).

The effect of wall emissivity is illustrated in Figs. 1 (a) and (b). From Fig. 1 (a), it is seen that the increase of wall emissivity will increase the heat flux losses at the hot face as well as the heat flux gains at the cold face. This can be easily understood by the fact that the emission and absorption of the wall is proportional to its wall emissivity. It is seen from Fig. 1 (b) that, with the increase of wall emissivity, the emissive power in the medium near the hot face ($x < 0$) increases. While a reverse effect near the cold face ($x > 0$) is found. A constant value of emissive power is found to be 0.1665 at $x = y = z = 0$ for various wall emissivities. It should be noted that all the walls have the same emissivity. The increase of emissive power near the hot face is due to the increase of heat losses at the hot face. In order to maintain

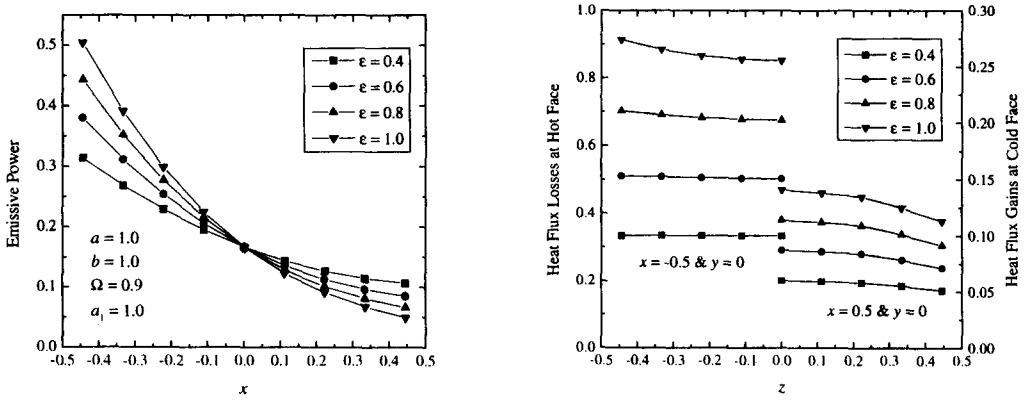

(a) (b)

FIG. 1

Effect of wall emissivity. (a) emissive power at $y = z = 0$; (b) radiative heat flux.

a heat balance, the emissive power of the medium near the hot face has to increase. The decrease of emissive power in the medium near the cold face is due to the fact that the emissive power at the hot face increases, but the emissive power at the cold face is always zero for all cases. This means that the emissive power gradient along the x-axis increases. Thus, a decreased emissive power is found in the medium near the cold face.

The influence of scattering albedo is discussed in Figs. 2 (a) and (b), in which the surface heat flux distributions at the hot face and cold face are displayed. A forward scattering medium is employed in Fig. 2 (a). It is seen that the increase of scattering albedo will increase the heat flux losses as well as the heat flux gains. This is because the increase of scattering albedo increases the forward scattering radiation. So that it is easier to transfer radiation energy from the hot face to the cold face, which results in the increase of surface heat flux. In the case of a backward scattering medium as in Fig. 2 (b), the radiation from the hot face will be reflected back by the medium. The increment of scattering albedo increases the reflected radiation, which results in the decrease of the surface heat flux.

The forward fraction f of scattering phase function also influences the radiative heat transfer. A positive value of f means a forward scattering, while a negative value represents a backward scattering. The larger the absolute value, the stronger the forward or backward scattering. The influence of f is inspected in Figs. 3 (a) and (b). From Fig. 3 (a), it is seen that, the stronger the forward scattering, the larger the heat flux. A strong backward scattering decreases the surface heat flux. These can be explained from Eq. (5), in which the scaled extinction coefficient decreases (or increases) with the increase (or decrease) of f. As a result, the heat flux increased (or decreased). The effect of f on the emissive power of the medium is demonstrated in Fig. 3 (b). It is found that, a forward scattering will decrease the emissive

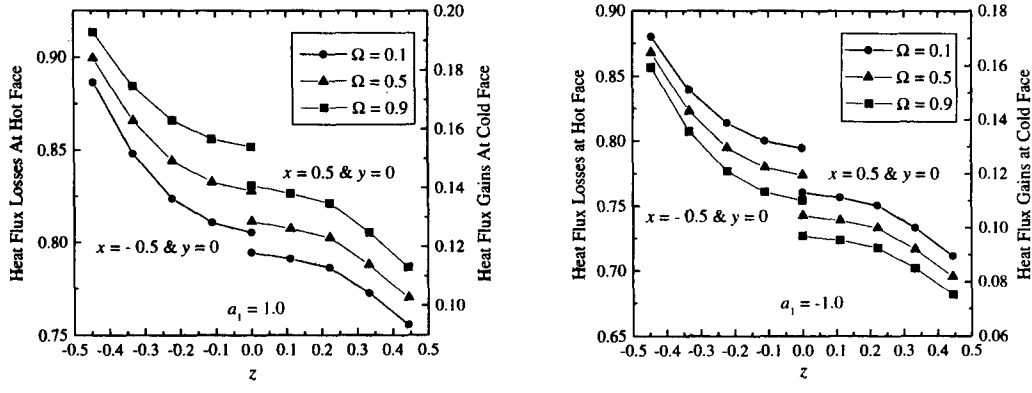

FIG. 2

Effect of scattering albedo. (a) forward scattering with $a_1 = 1$; (b) backward scattering with $a_1 = -1$.

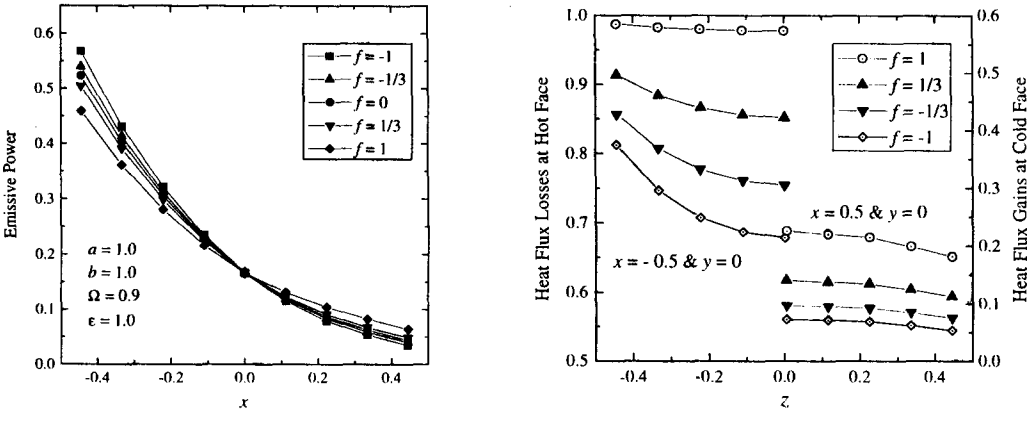

FIG. 3

Effect of forward fraction of phase function. (a) emissive power at $y = z = 0$; (b) radiative heat flux.

power of the medium near the hot face, but increase the emissive power of the medium near the cold face. The effects for the backward scattering medium are reversed.

For a cubic gray medium in radiative equilibrium with black isothermal walls, the temperature at the center of the cube is analyzed by Crosbie and Schrenker [16] and can be expressed by

$$T_0^4 = \sum_{i=1}^{6} T_i^4 / 6 \tag{15}$$

in which, T_0 is the temperature at the center of the cube and T_i's (i = 1 to 6) are the temperatures at six walls. We found that the above relationship is valid for nonhomogeneous cubic medium if the extinction

coefficient profile is axisymmetric. Equation (15) is also valid for gray diffuse isothermal walls if all the walls have the same radiational property. Table 5 summarizes some representative calculations. Equation (15) may be valid for anisotropic scattering medium since the scaled isotropic results at the cube center are in excellent consistency with the anisotropic predictions in the previous bench mark problems. However, a further analysis is necessary.

TABLE 5

Comparison of calculated and analyzed temperatures at the center of cubic nonhomogeneous media.

σT_1^4	σT_2^4	σT_3^4	σT_4^4	σT_5^4	σT_6^4	σT_0^4 (calculated)	σT_0^4 (exact)
1	0	0	0	0	0	0.1665 ± 0.0005	1/6
1	1	0	0	0	0	0.3337 ± 0.0005	1/3
1	1	0.5	0	0	0	0.4172 ± 0.0005	5/12
1	0.5	0.5	0.5	0	0	0.4165 ± 0.0005	5/12
1	0.8	0.6	0.4	0.2	0	0.5003 ± 0.0005	1/2
1	1	1	0.5	0.5	0.5	0.7500 ± 0.0005	3/4

Conclusions

The scaled isotropic scattering radiative heat transfer in a three-dimensional nonhomogeneous medium is numerically investigated. The scaled isotropic results are compared with the anisotropic scattering results. A good agreement is found between these two approaches. The radiative heat transfer is strongly influenced by the radiative property parameters such as the wall emissivity, scattering albedo and forward fraction of phase function. The surface radiative heat flux increases with the increases of the forward fraction of phase function and the wall emissivity. With the increase of scattering albedo, the radiative heat flux increases for forward scattering media, while a decrease of heat flux is found for backward scattering media. The emissive power in the medium near hot face increases with the increase of wall emissivity or the decrease of forward fraction. However, a reverse effect was found in the medium near the cold face. The temperature at the center of a cubical nonhomogeneous medium in radiative equilibrium with gray diffuse walls can be analyzed by the relationship of equation (15).

Nomenclature

A_i^R	effective radiation area, Eq. (9)
E_b	blackbody emissive power
f	forward fraction of phase function, Eq. (2)
$F_{i,j}^A$	absorption view factor from element i to j

$F_{i,j}^{D}$	diffuse scattering view factor from element i to j
I	radiation intensity
Q_T	heat transfer rate of emissive power
Q_J	heat transfer rate of diffuse radiosity, Eq. (10)
Q_X	net heat transfer rate of heat generation, Eq. (11)
S	path length through an element
T	temperature
x,y,z	Cartesian coordinates
β	extinction coefficient
ε	emissivity, $\equiv 1-\Omega^{D}-\Omega^{S}$
Φ	scattering phase function
Ω^{D}	albedo of a volume element or diffuse reflectivity of a surface element
Ω^{S}	specular reflectivity
ω	solid angle
σ	Stefan-Boltzmann constant

References

1. T.-K. Kim and H.S. Lee, *ASME J. Heat Transfer*, 112, 721 (1990).
2. H. Lee and R.O. Buchius, *ASME J. Heat Transfer*, 104, 68 (1982).
3. W.J. Wiscombe, *J. Atmosp. Sciences*, 34, 1408 (1977).
4. J.H. Joseph, W.J. Wiscombe and J.A. Weinman, *J. Atmosp. Sciences*, 33, 2452 (1976).
5. B.H.J. McKellar and M.A. Box, *J. Atmosp. Sciences*, 38, 1063 (1981).
6. S. Maruyama, *Int. J. Heat Mass Transfer*, 41, 2847 (1998).
7. J.C. Chai, H.S. Lee and S.V. Patankar, *Numerical Heat Transfer, Part B*, 24, 373 (1993).
8. S. Maruyama, *Numerical Heat Transfer, Part A*, 24, 181 (1993).
9. S. Maruyama and T. Aihara, *ASME J. Heat Transfer*, 119, 129 (1997).
10. S. Maruyama and M. Higano, *Energy Conversion and Management*, 38, 1187 (1997).
11. Z. Guo, S. Maruyama and T. Tsukada, *Numerical Heat Transfer, Part A*, 32, 595 (1997).
12. Z. Guo, S. Maruyama and S. Togawa, *J. Crystal Growth*, 194, 321 (1998).
13. S. Maruyama, Z. Guo and M. Higano, Proc. 11th Int. Heat Transfer Conf., Korea, 7, 457 (1998).
14. Z. Guo and S. Maruyama, ASME PVP-Vol. 377-2, p. 101 (1998).
15. P.F. Hsu and J.T. Farmer, *ASME J. Heat Transfer*, 119, 185 (1997).
16. A.L. Crosbie and R.G. Schrenker, *J. Quant. Spectrosc. Radiat. Transfer*, 28, 507 (1982).

Received May 7, 1999